

hep-ph/9801329

CERN-TH/98-11
DFPD 98/TH/04

Signals of a superlight gravitino at hadron colliders when the other superparticles are heavy ¹

Andrea Brignole ^{a,b,2}, Ferruccio Feruglio ^{a,b,c,3},Michelangelo L. Mangano ^{c,4,5} and Fabio Zwirner ^{a,b,6}^a Istituto Nazionale di Fisica Nucleare, Sezione di Padova, I-35131 Padua, Italy^b Dipartimento di Fisica, Università di Padova, I-35131 Padua, Italy^c Theory Division, CERN, CH-1211 Geneva 23, Switzerland

Abstract

If the gravitino \tilde{G} is very light and all the other supersymmetric particles are above threshold, supersymmetry may still be found at colliders, by looking at processes with only gravitinos and ordinary particles in the final state. We compute here the cross-sections for some distinctive signals at hadron colliders: photon plus missing energy, induced by $q\bar{q} \rightarrow \tilde{G}\tilde{G}\gamma$, and jet plus missing energy, induced by $q\bar{q} \rightarrow \tilde{G}\tilde{G}g$, $qg \rightarrow \tilde{G}\tilde{G}q$, $\bar{q}g \rightarrow \tilde{G}\tilde{G}\bar{q}$ and $gg \rightarrow \tilde{G}\tilde{G}g$. From the present Tevatron data, we estimate the bound $m_{3/2} > 2.7 \times 10^{-5}$ eV on the gravitino mass, corresponding to the bound $\sqrt{F} > 335$ GeV on the supersymmetry-breaking scale. We foresee that the upgraded Tevatron and the LHC will be sensitive to values of $m_{3/2}$ up to 4.9×10^{-5} eV and 1.2×10^{-3} eV, corresponding to \sqrt{F} up to 450 GeV and 2.2 TeV, respectively.

CERN-TH/98-11
January 1998

¹Work supported in part by the European Commission TMR Programme ERBFMRX-CT96-0045.

²e-mail address: brignole@pd.infn.it

³e-mail address: feruglio@pd.infn.it

⁴On leave of absence from: Istituto Nazionale di Fisica Nucleare, Sezione di Pisa, I-56100 Pisa, Italy.

⁵e-mail address: mlm@vxcern.cern.ch

⁶e-mail address: zwirner@pd.infn.it

1 Introduction

While there are strong theoretical motivations for supersymmetry, with supersymmetry-breaking mass splittings of the order of the electroweak scale (for reviews and references, see e.g. [1]), there is at present no compelling argument to select a definite value of the supersymmetry-breaking scale \sqrt{F} or, equivalently¹, the gravitino mass $m_{3/2}$. As reviewed in [2], different possibilities should then be kept in mind when performing phenomenological analyses: they are characterized by a ‘heavy’, ‘light’ or ‘superlight’ gravitino. In the heavy gravitino case, reactions involving the gravitino are never important for collider physics. In the light gravitino case, the gravitino can be relevant in the decays of other supersymmetric particles, if there is sufficient energy to produce the latter. In the superlight gravitino case, also the direct production of gravitinos (with or without other supersymmetric particles) can become relevant. In this paper, we concentrate on the superlight gravitino case, where \sqrt{F} can be close to the electroweak scale and, correspondingly, $m_{3/2}$ can be several orders of magnitude below the eV scale.

Many aspects of the superlight gravitino phenomenology at colliders have been discussed long ago [3], and also more recently [4]. In all these papers, however, it was assumed that some other supersymmetric particle, for example a neutralino or one of the spin-0 partners of the gravitino, is light enough to be produced on-shell in some reaction. Here we take an orthogonal point of view: there may be experiments where the available energy is still insufficient for the on-shell production of other supersymmetric particles, but nevertheless sufficient to give rise to final states with only gravitinos and ordinary particles, at measurable rates. In a recent paper [5], some of us considered the process $e^+e^- \rightarrow \tilde{G}\tilde{G}\gamma$, which may give rise to a distinctive *photon + missing energy* signal at e^+e^- colliders. In the present work, we study the possible signals of a superlight gravitino at hadron colliders, such as the Tevatron or the LHC. At the partonic level, we consider the following subprocesses:

$$q + \bar{q} \rightarrow \tilde{G} + \tilde{G} + \gamma, \quad (1)$$

$$q + \bar{q} \rightarrow \tilde{G} + \tilde{G} + g, \quad (2)$$

$$q + g \rightarrow \tilde{G} + \tilde{G} + q, \quad (3)$$

$$\bar{q} + g \rightarrow \tilde{G} + \tilde{G} + \bar{q}, \quad (4)$$

$$g + g \rightarrow \tilde{G} + \tilde{G} + g. \quad (5)$$

The process of eq. (1) corresponds to a *photon + missing transverse energy (E_T)* signal, those of eqs. (2)–(5) to a *jet + E_T* signal. We compute the cross-section and the relevant angular distributions for the processes of eqs. (1)–(5), in the limit in which the supersymmetric particles of the Minimal Supersymmetric Standard Model (MSSM), such as squarks and gauginos, and all other exotic particles, such as the spin-0 partners of the goldstino, are heavy. We then analyse the resulting phenomenology at the Tevatron ($p\bar{p}$, $\sqrt{S} = 1.8$ TeV, $L \sim 100 \text{ pb}^{-1}$), the upgraded Tevatron ($p\bar{p}$, $\sqrt{S} = 2$ TeV, $L \sim 2 \text{ fb}^{-1}$), and

¹We recall that, in a flat space-time, $F = \sqrt{3} m_{3/2} M_P$, where $M_P = (8\pi G_N)^{-1/2} \simeq 2.4 \times 10^{18} \text{ GeV}$ is the Planck mass. Note that we take F real and positive, which is not restrictive for the present paper.

the LHC (pp , $\sqrt{S} = 14$ TeV, $L \sim 10 \text{ fb}^{-1}$). We show how the present Tevatron data, in the absence of a signal over the Standard Model background, should allow us to establish the lower bound $\sqrt{F} \gtrsim 335$ GeV, or, equivalently, $m_{3/2} \gtrsim 2.7 \times 10^{-5}$ eV. These bounds are considerably better than the one estimated [5] from the present LEP data, $\sqrt{F} \gtrsim 200$ GeV or $m_{3/2} \gtrsim 10^{-5}$ eV. We also estimate the future sensitivity of the upgraded Tevatron and the LHC: \sqrt{F} up to 450 GeV and 2.2 TeV, corresponding to $m_{3/2}$ up to 4.9×10^{-5} eV and 1.2×10^{-3} eV, respectively. In contrast with other collider bounds discussed in the literature [4], those discussed in the present paper cannot be evaded by modifying the mass spectrum of the other supersymmetric particles: making some additional supersymmetric particle light leads in general to stronger bounds. Therefore, making use of our results, an *absolute* lower bound on the gravitino mass can be established.

The paper is organized as follows. In sect. 2, we spell out and discuss the low-energy effective Lagrangian used for our calculations. In sect. 3, we compute the relevant differential cross-sections at the partonic level. In sects. 4 and 5, we discuss the phenomenology of the jet + \cancel{E}_T and $\gamma + \cancel{E}_T$ signals at hadron colliders, emphasizing the implications of the present Tevatron data and the prospects for the upgraded Tevatron and the LHC. Finally, in sect. 6 we summarize and discuss our results.

2 The effective Lagrangian

For the theoretically oriented readers, we summarize the framework of our calculation. We are considering processes whose typical energies are much larger than the gravitino mass, but smaller than the masses of all the other particles not belonging to the Standard Model. We can then work with the low-energy effective theory defined by the following two-step procedure. We start from a generic supergravity Lagrangian, assuming that supersymmetry is spontaneously broken with a light gravitino, and we take the appropriate low-energy limit: $M_P \rightarrow \infty$ with \sqrt{F} fixed. In accordance with the supersymmetric equivalence theorem [6], gravitational interactions are consistently neglected in this limit, and we end up with an effective (non-renormalizable) theory with linearly realized, although spontaneously broken, global supersymmetry, whose building blocks are the chiral and vector supermultiplets containing the light degrees of freedom, including the goldstino. To simplify the discussion, we assume that such a theory has pure F -breaking and negligible higher-derivative terms. Since we are interested in the case where the available energy is smaller than the supersymmetry-breaking mass splittings, we perform a second step and move to a ‘more effective’ theory, by explicitly integrating out the heavy superpartners in the low-energy limit. The only degrees of freedom left are then the goldstino and the Standard Model particles, and supersymmetry is non-linearly realized [7, 8, 9].

The derivation of the low-energy effective Lagrangian, to be used as the starting point for our calculations, proceeds exactly as in [5]. The only differences are that now the unbroken gauge group is $SU(3)_C \times U(1)_{em}$ and that we are dealing with quarks instead of leptons. In analogy with [5], we neglect the light quark masses and any possible mixing in the squark sector. Denoting with q^α the light quark fields (where $\alpha = 1, 2, 3$ and

$q = u, d, s, c, b$), and with $(A_\mu)_\beta^\alpha \equiv A_\mu^A (T^A)_\beta^\alpha$ the gluon fields (where $A = 1, \dots, 8$ and T^A are the $SU(3)_C$ generators), the covariant derivative with respect to $SU(3)_C \times U(1)_{em}$ reads:

$$(D_\mu)_\beta^\alpha = (\partial_\mu - ieQ_q A_\mu) \delta_\beta^\alpha - ig_S (A_\mu)_\beta^\alpha. \quad (6)$$

Focusing only on the terms relevant for our calculations, we obtain:

$$\mathcal{L}_{eff} = -\frac{1}{4} F_{\mu\nu} F^{\mu\nu} - \frac{1}{4} F_{\mu\nu}^A F^{\mu\nu A} + i \sum_q \bar{q}_\alpha (\not{D})_\beta^\alpha q^\beta + \frac{i}{2} \bar{\tilde{G}} \not{\partial} \tilde{G} + \sum_{i=1}^4 \mathcal{O}_i. \quad (7)$$

The terms \mathcal{O}_i ($i = 1, \dots, 4$) are local operators, bilinear in the goldstino and generated by the exchange of massive particles in the large-mass limit. Their field-dependent parts have mass dimension $d = 8$, and the corresponding coefficients scale as $1/F^2$. The operator \mathcal{O}_1 involves only vector bosons (photons or gluons) and goldstinos, and is generated [2] by integrating over the spin-0 partners of the goldstino and the gauginos:

$$\mathcal{O}_1 = -\frac{i}{64F^2} \left(\bar{\tilde{G}} [\gamma^\mu, \gamma^\nu] F_{\mu\nu} \not{\partial} [\gamma^\rho, \gamma^\sigma] F_{\rho\sigma} \tilde{G} + \bar{\tilde{G}} [\gamma^\mu, \gamma^\nu] F_{\mu\nu}^A (\not{D})^{AB} [\gamma^\rho, \gamma^\sigma] F_{\rho\sigma}^B \tilde{G} \right), \quad (8)$$

where \not{D} is constructed with the covariant derivative in the adjoint representation. The operator \mathcal{O}_2 is a four-fermion interaction among quarks and goldstinos, recovered by combining a contact term in the original Lagrangian with contributions originating from squark exchanges [8]:

$$\mathcal{O}_2 = -\frac{1}{2F^2} \left\{ \bar{q}_\alpha \tilde{G} \square \left(\bar{\tilde{G}} q^\alpha \right) - \bar{q}_\alpha \gamma_5 \tilde{G} \square \left(\bar{\tilde{G}} \gamma_5 q^\alpha \right) \right\}. \quad (9)$$

The operator \mathcal{O}_3 is generated by attaching a photon or a gluon to a squark exchanged among quarks and goldstinos:

$$\mathcal{O}_3 = \frac{i}{F^2} \sum_q \left[eQ_q A^\mu \delta_\beta^\alpha + g_s (A_\mu)_\beta^\alpha \right] \left\{ \bar{q}_\alpha \tilde{G} \partial_\mu \left(\bar{\tilde{G}} q^\beta \right) - \bar{q}_\alpha \gamma_5 \tilde{G} \partial_\mu \left(\bar{\tilde{G}} \gamma_5 q^\beta \right) \right\}. \quad (10)$$

The operators \mathcal{O}_2 and \mathcal{O}_3 are not gauge invariant, but their sum is contained in a gauge-invariant combination, as can easily be verified. Finally, the operator \mathcal{O}_4 is a gauge-invariant contact term that directly contributes (as \mathcal{O}_3) to the scattering amplitudes of eqs. (1)–(4). It originates from a combined squark and gaugino exchange:

$$\begin{aligned} \mathcal{O}_4 = & -\frac{i}{8F^2} \left[eQ_q F_{\mu\nu} \delta_\beta^\alpha + g_s F_{\mu\nu}^A (T^A)_\beta^\alpha \right] \left\{ \bar{\tilde{G}} [\gamma^\mu, \gamma^\nu] \left(q^\beta \bar{q}_\alpha \tilde{G} - \gamma_5 q^\beta \bar{q}_\alpha \gamma_5 \tilde{G} \right) \right. \\ & \left. + \left(\bar{\tilde{G}} q^\beta \bar{q}_\alpha - \bar{\tilde{G}} \gamma_5 q^\beta \bar{q}_\alpha \gamma_5 \right) [\gamma^\mu, \gamma^\nu] \tilde{G} \right\}. \end{aligned} \quad (11)$$

As a final remark, we should mention that the processes considered in the present paper were also considered in [10], in the same kinematical limit, but relying on the effective Lagrangian traditionally associated with the standard non-linear realization of supersymmetry [7], which was believed at that time to be unique at leading order. As was recently emphasized [8], however, such an approach is not equivalent to ours, and the two lead to different results, both consistent with supersymmetry. For a model-independent study, we would need the general form of the low-energy effective interactions, allowed by the

non-linearly realized supersymmetry, that may contribute to the relevant amplitudes at leading order. This was not known until recently, when a definite theoretical prescription for such an investigation became available [9] (the same paper also confirmed the results of [8], and found the explicit general form of the coupling of two on-shell goldstinos to a single photon). We are postponing a general phenomenological analysis to a forthcoming paper. Because of the strong and universal power-law behaviour of the cross-sections, always proportional to s^3/F^4 , we expect our results to be rather stable with respect to variations of the parameters characterizing the most general non-linear realization. However, should a signal show up at the Tevatron or the LHC, having the general expression of the cross-section would be very important, since a detailed analysis of the spectrum and of the angular distributions of photons, jets and missing energy would offer the unique opportunity of distinguishing among possible fundamental theories.

3 Partonic cross-sections

We now compute the cross-sections for the processes of eqs. (1)–(4), and comment on the cross-section for the process of eq. (5).

For the process $q\bar{q} \rightarrow \tilde{G}\tilde{G}\gamma$, the calculation is a trivial extension of the one performed in [5] for $e^+e^- \rightarrow \tilde{G}\tilde{G}\gamma$. We give here, for future use, a compact expression for the matrix element squared, summed over the helicities of the initial and final states. The calculation has been performed both by standard trace techniques, with the help of the program Tracer [11], and by helicity-amplitude techniques [12]. We denote by (p_1, p_2, q_1, q_2, k) the four-momenta of the incoming quark and antiquark and of the outgoing gravitinos and photon, respectively. For any given quark flavour, the result is

$$\langle |M(q\bar{q} \rightarrow \tilde{G}\tilde{G}\gamma)|^2 \rangle = \frac{Q_q^2 \alpha}{N} \frac{32\pi}{F^4(k \cdot p_1)(k \cdot p_2)(p_1 \cdot p_2)} \times [A(p_1, p_2, q_1, q_2, k) + A(p_2, p_1, q_1, q_2, k) + (q_1 \leftrightarrow q_2)] , \quad (12)$$

where the symbol $\langle \dots \rangle$ denotes the average (sum) over colours and helicities of the initial (final) state, Q_q is the electric charge of the quark under consideration, $\alpha \equiv e^2/(4\pi)$ is the electromagnetic fine-structure constant, $N = 3$ is the number of colours and

$$\begin{aligned} A(p_1, p_2, q_1, q_2, k) = & (kp_1)(kp_2)^2(kq_1)(p_1p_2)(p_1q_2) + (kp_1)(kp_2)(kq_1)^2(p_1p_2)(p_1q_2) \\ & + (kp_1)(kp_2)^2(kq_1)(p_1q_1)(p_1q_2) + (kp_1)(kp_2)(kq_1)^2(p_1q_1)(p_1q_2) \\ & + 2(kp_1)(kp_2)(kq_1)(p_1p_2)(p_1q_2)^2 + (kp_1)(kq_1)^2(p_1p_2)(p_1q_2)^2 \\ & + (kp_1)(kp_2)(kq_1)(p_1q_1)(p_1q_2)^2 - (kp_1)^2(kp_2)(kq_1)(p_1q_2)(p_2q_1) \\ & + (kp_2)(kq_2)(p_1p_2)(p_1q_1)(p_1q_2)(p_2q_1) + (kp_2)(kq_2)(p_1q_1)^2(p_1q_2)(p_2q_1) \\ & - (kp_1)^2(kq_1)(p_1q_2)^2(p_2q_1) - (kp_2)(kq_1)(p_1p_2)(p_1q_2)^2(p_2q_1) \\ & - (kp_2)(kq_1)(p_1q_1)(p_1q_2)^2(p_2q_1) - (kp_1)(kq_2)(p_1q_1)(p_1q_2)(p_2q_1)^2 \end{aligned}$$

$$\begin{aligned}
& + (kp_2)(kq_2)(p_1p_2)(p_2q_1)^3 - (kq_2)(p_1p_2)(p_1q_2)(p_2q_1)^3 \\
& + (kp_1)(kq_1)(p_1q_1)(p_1q_2)(p_2q_1)(p_2q_2) + (kq_1)(p_1p_2)(p_1q_2)(p_2q_1)^2(p_2q_2) \\
& - (kp_1)(kp_2)(p_1p_2)(p_1q_2)(p_2q_1)(q_1q_2) - (kp_1)(kq_1)(p_1p_2)(p_1q_2)(p_2q_1)(q_1q_2) \\
& - (kp_1)(kp_2)(p_1q_1)(p_1q_2)(p_2q_1)(q_1q_2) + (kp_1)^2(p_1q_2)(p_2q_1)^2(q_1q_2) \\
& - (kp_2)(p_1p_2)(p_1q_2)(p_2q_1)^2(q_1q_2) + (p_1p_2)(p_1q_2)^2(p_2q_1)^2(q_1q_2) . \tag{13}
\end{aligned}$$

After integrating over part of the phase space, we obtain:

$$\frac{d^2\sigma}{dx_\gamma d\cos\theta_\gamma} = \frac{Q_q^2\alpha}{N} \frac{s^3}{160\pi^2 F^4} \cdot f(x_\gamma, \cos\theta_\gamma) , \tag{14}$$

where $(\sqrt{s}, x_\gamma, \theta_\gamma)$ are the total energy, the fraction of beam energy carried by the photon, and the photon scattering angle with respect to the quark, in the centre-of-mass frame of the incoming partons. The function f is given by [5]

$$f(x_\gamma, \cos\theta_\gamma) = \frac{(1-x_\gamma)^3(2-2x_\gamma+x_\gamma^2)}{x_\gamma \sin^2\theta_\gamma} \tag{15}$$

$$+ \frac{1}{48}x_\gamma(-138 + 354x_\gamma - 251x_\gamma^2 + 72x_\gamma^3 + 3x_\gamma^4) + \frac{1}{96}x_\gamma^3(37 - 74x_\gamma - 3x_\gamma^2) \sin^2\theta_\gamma .$$

The extension to the process $q\bar{q} \rightarrow \tilde{G}\tilde{G}g$ is straightforward, since the only difference is the replacement of the photon with the gluon. By replacing $Q_q^2\alpha$ with $C_F\alpha_S$ in eqs. (12) and (14), where $C_F = (N^2 - 1)/2N = 4/3$, we obtain:

$$\frac{d^2\sigma}{dx_g d\cos\theta_g} = \frac{C_F\alpha_S}{N} \frac{s^3}{160\pi^2 F^4} \cdot f(x_g, \cos\theta_g) . \tag{16}$$

For the crossed channels, $qg \rightarrow \tilde{G}\tilde{G}q$ ($\bar{q}g \rightarrow \tilde{G}\tilde{G}\bar{q}$), analogous results can easily be obtained by taking eqs. (12) and (13), by replacing $Q_q^2\alpha/N$ with $C_F\alpha_S/(N^2 - 1)$, by performing the substitution $k \leftrightarrow -p_2$ ($k \leftrightarrow -p_1$), and by changing the overall sign. After integrating over part of the phase space, we easily obtain the one-parton inclusive distributions in terms of the partonic centre-of-mass beam-energy fraction $x_q(x_{\bar{q}})$ and scattering angle $\theta_q(\theta_{\bar{q}})$. For the $qg \rightarrow \tilde{G}\tilde{G}q$ channel:

$$\frac{d\sigma}{dx_q d\cos\theta_q} = \frac{C_F\alpha_S}{N^2 - 1} \frac{s^3}{160\pi^2 F^4} g(x_q, \cos\theta_q) , \tag{17}$$

where θ_q is the angle between the direction of the incoming and outgoing quarks, and

$$\begin{aligned}
g(x_q, \cos\theta_q) &= \frac{(1-x_q)^3}{16\sin^2(\theta_q/2)} \frac{1+x_q^2}{1-x_q} + \frac{(1-x_q)^3}{4\cos^2(\theta_q/2)} [(1-x_q)^2 + x_q^2] \\
&+ \frac{x_q}{96} [156 - (373 - 189\cos\theta_q)x_q + 2(277 - 155\cos\theta_q)x_q^2] \\
&- (323 - 103\cos\theta_q + 10\cos^2\theta_q + 10\cos^3\theta_q)x_q^3 + 2(3 - \cos\theta_q)x_q^4 . \tag{18}
\end{aligned}$$

Because of the obvious symmetry properties of eq. (12), an identical expression is obtained for the $\bar{q}g \rightarrow \tilde{G}\tilde{G}\bar{q}$ channel.

It is easy to verify that all the above results satisfy the required factorization properties in the case of collinear emission:

$$\frac{d\sigma}{dx_g d\cos\theta_g}(q\bar{q} \rightarrow \tilde{G}\tilde{G}g) \xrightarrow{g\parallel q} \sigma(q\bar{q} \rightarrow \tilde{G}\tilde{G}; (1-x_g)s) \frac{\alpha_S}{\pi} \frac{1}{\sin^2\theta_g} P_{gg}(x_g), \quad (19)$$

$$\frac{d\sigma}{dx_q d\cos\theta_q}(qg \rightarrow \tilde{G}\tilde{G}q') \xrightarrow{q'\parallel q} \sigma(gg \rightarrow \tilde{G}\tilde{G}; (1-x_q)s) \frac{\alpha_S}{\pi} \frac{1}{4\sin^2(\theta_q/2)} P_{qq}(x_q), \quad (20)$$

$$\frac{d\sigma}{dx_q d\cos\theta_q}(qg \rightarrow \tilde{G}\tilde{G}q') \xrightarrow{q'\parallel g} \sigma(q\bar{q} \rightarrow \tilde{G}\tilde{G}; (1-x_q)s) \frac{\alpha_S}{\pi} \frac{1}{4\cos^2(\theta_q/2)} P_{qg}(x_q), \quad (21)$$

where P_{ij} are the standard Altarelli-Parisi splitting kernels, and

$$\sigma(q\bar{q} \rightarrow \tilde{G}\tilde{G}; s) = \frac{1}{N} \frac{s^3}{160\pi F^4}, \quad (22)$$

$$\sigma(gg \rightarrow \tilde{G}\tilde{G}; s) = \frac{1}{N^2 - 1} \frac{s^3}{640\pi F^4}. \quad (23)$$

We did not perform the complete calculation of the $gg \rightarrow \tilde{G}\tilde{G}g$ process, since the contribution of the gg channel is significantly suppressed at the highest values of s , where the signal is more likely to emerge over the QCD backgrounds. To verify this statement, we shall use in the next section an approximate estimate of the gg process, based on the collinear approximation:

$$\frac{d\sigma}{dx_g d\cos\theta_g}(gg \rightarrow \tilde{G}\tilde{G}g) \sim \sigma(gg \rightarrow \tilde{G}\tilde{G}; (1-x_g)s) \frac{\alpha_S}{\pi} \frac{1}{\sin^2\theta_g} P_{gg}(x_g). \quad (24)$$

Our results will confirm that indeed the contribution of this channel is strongly suppressed in the kinematical regions of interest.

4 The jet-plus-missing-energy signal

In this section, we evaluate the rates for the production of a single jet of large transverse energy (E_T) plus a gravitino pair in hadronic collisions. We shall consider the cases of the currently available Tevatron data (TeV I, $p\bar{p}$ collisions at $\sqrt{S} = 1.8$ TeV, with an integrated luminosity of approximately 100 pb^{-1}), of the upcoming upgraded Tevatron run (TeV II, $p\bar{p}$ collisions at $\sqrt{S} = 2$ TeV, with an integrated luminosity of approximately 2 fb^{-1}), and of the LHC (pp collisions at $\sqrt{S} = 14$ TeV, with an integrated luminosity of approximately 10 fb^{-1}). The dominant irreducible background to the signal comes from the associated production of a Z vector boson and a jet, with the Z decaying to a neutrino pair. Given the large values of E_T we will be considering (in excess of 100 GeV), no significant detector backgrounds are expected. Notice that the standard experimental searches of supersymmetry using multi-jet-plus- \cancel{E}_T final states require the presence of at least three jets. No experimental study has been published, to date, of the single-jet-plus- \cancel{E}_T signal discussed here. As a result we have to rely on our own background estimate, since nothing is available from the experimental studies. We shall therefore extract the

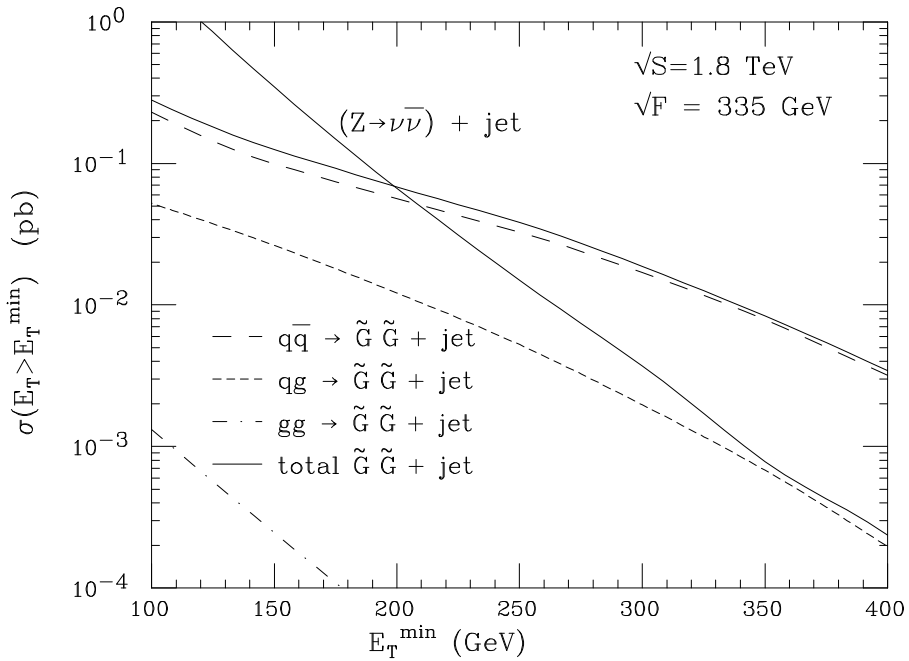


Figure 1: Production rates for $p\bar{p} \rightarrow \tilde{G}\tilde{G} + \text{jet}$ and $p\bar{p} \rightarrow \text{jet} + \nu\bar{\nu}$ at $\sqrt{S} = 1.8$ TeV.

region of sensitivity to the value of the scale \sqrt{F} from the comparison of the expected signal and the calculated background rates.

In our numerical analysis, we shall use the parton-density parametrization MRSR2 [13], with a renormalization/factorization scale $\mu = E_T$. Since the cross-sections for both signal and background processes scale linearly with α_S , their ratio is rather insensitive to this choice. In particular, since the signal rate is proportional to F^{-4} , the limits we shall set on \sqrt{F} are not significantly affected by this choice, as we have explicitly verified by varying the scale μ in the range $E_T/4 < \mu < 4E_T$, independently for signal and background.

Figures 1–3 show the contribution to the signal rate of the three possible initial states $q\bar{q}$, $qg + gq$ and gg . The distributions shown correspond to the jet rate integrated over transverse energies larger than a given threshold E_T^{\min} , and within a jet-rapidity range $|\eta| < 2.5$. For the three figures we selected the values of $\sqrt{F} = 335, 450$, and 2200 GeV, respectively. This particular choice will be justified later on. The relative contributions of the three channels and the shapes of their distributions are not affected by the value of \sqrt{F} . For comparison, we also show the background rate for the process $p\bar{p} \rightarrow Z \text{ jet} \rightarrow \nu\bar{\nu} \text{ jet}$. This was calculated at leading order in QCD. The capability of LO QCD to describe this process is proved by the recent study of the Z -plus-multiparticle final states published by CDF [14], with the Z decaying to charged lepton pairs. In this paper the ratio Data/Theory for the Z -plus-1-jet final state was found to be 1.29 ± 0.17 , using $\mu = E_T$. For consistency with this result, we rescaled our LO background prediction by a factor 1.29. To be conservative, however, we did not rescale the signal rates.

We emphasize the following features of these distributions. First of all, notice that the shape of the background is much steeper than that of the signal. This is due to the

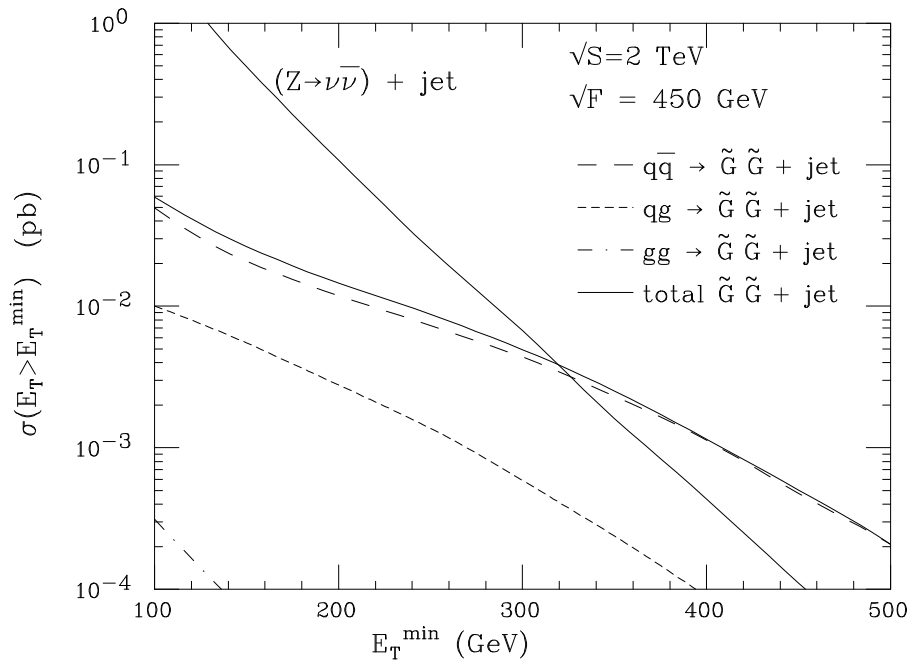


Figure 2: Production rates for $p\bar{p} \rightarrow \tilde{G}\tilde{G} + \text{jet}$ and $p\bar{p} \rightarrow \text{jet} + \nu\bar{\nu}$ at $\sqrt{S} = 2 \text{ TeV}$.

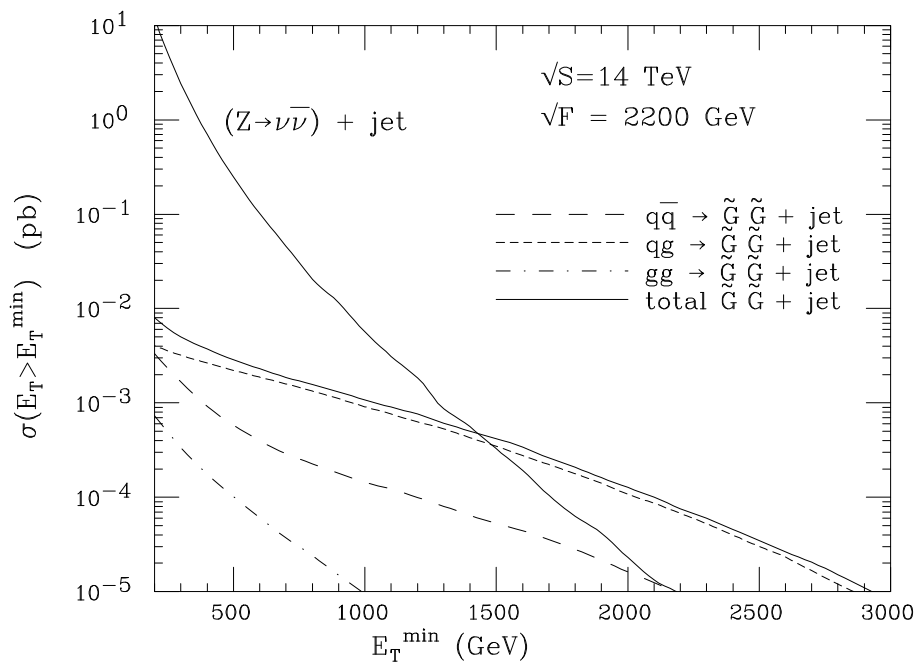


Figure 3: Production rates for $pp \rightarrow \tilde{G}\tilde{G} + \text{jet}$ and $pp \rightarrow \text{jet} + \nu\bar{\nu}$ at $\sqrt{S} = 14 \text{ TeV}$.

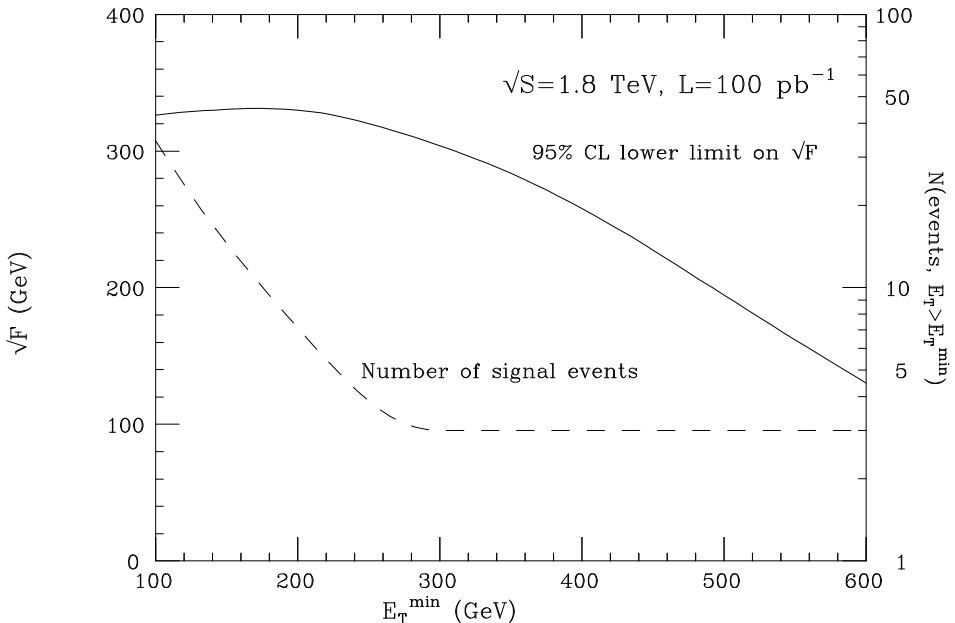


Figure 4: Solid line (scale on the left axis): estimated 95% CL exclusion limits on \sqrt{F} from the absence of a deviation from the SM jet+ E_T rate in events with jet- $E_T > E_T^{\min}$ at TeV I. Dashed line (scale on the right axis): number of jet+ $\tilde{G}\tilde{G}$ events with jet- $E_T > E_T^{\min}$ corresponding to the 95% CL value of \sqrt{F} .

high-energy enhancement caused by the s^3 behaviour of the signal cross-section, which strongly tempers the rapid fall off of the parton luminosities at large s . This suggests that the best limit on \sqrt{F} will be extracted from a comparison of signal and background in the region of high E_T , where the background is smallest. Secondly, notice that the contribution of the gg initial state is always negligible in the interesting regions of E_T , due to the smallness of the gluon density compared with the valence quark density. This is true regardless of the collider energy and justifies our use of an approximate expression for the $gg \rightarrow \tilde{G}\tilde{G}g$ matrix elements. Finally, notice that while at the Tevatron the signal is dominated by the $q\bar{q}$ initial state, the dominant contribution at the LHC comes from the $qg + gq$ channel. This is because the antiquark density in pp collisions is much smaller than the gluon density.

To extract the region of sensitivity to the scale \sqrt{F} , we count the number of background events expected above a given threshold E_T^{\min} and evaluate the value of \sqrt{F} that can be excluded at the 95% confidence level (CL). For values of E_T^{\min} such that no more background events are expected, this corresponds to a limit of 3 signal events. The 95% CL lower limits on \sqrt{F} for the three cases considered are plotted as functions of E_T^{\min} in figs. 4–6. In the same figures we also plotted (as dashed lines) the number of signal events corresponding to the selected value of \sqrt{F} . The best limits on \sqrt{F} that can be extracted with the chosen integrated luminosities are given by 335, 450 and 2200 GeV for TeV I, TeV II and the LHC, respectively. The corresponding limits on $m_{3/2}$ are 2.7×10^{-5} eV, 4.9×10^{-5} eV and 1.2×10^{-3} eV. These limits are obtained for values of E_T^{\min} just below the

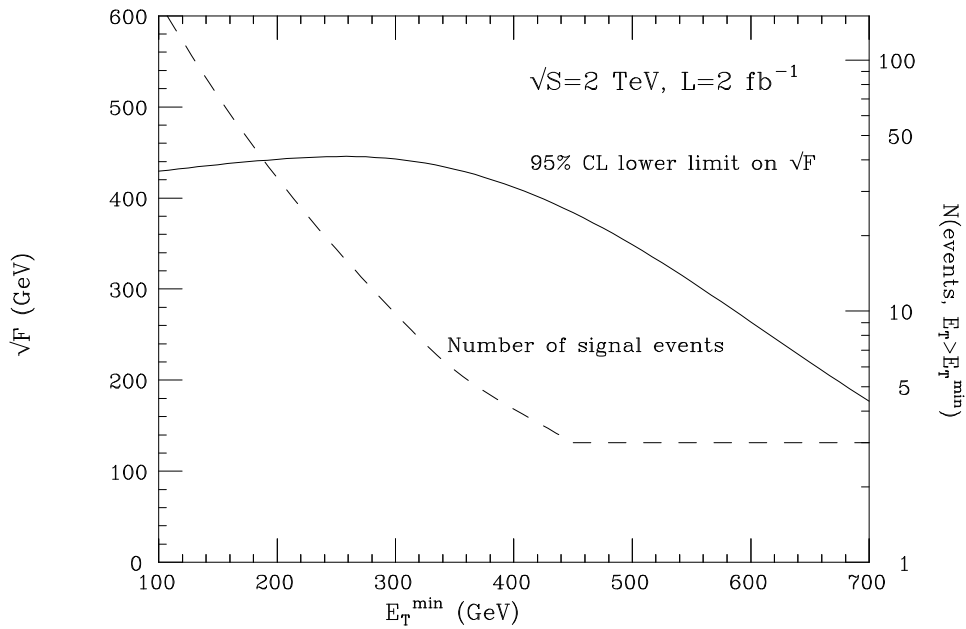


Figure 5: Same as fig. 4, for TeV II.

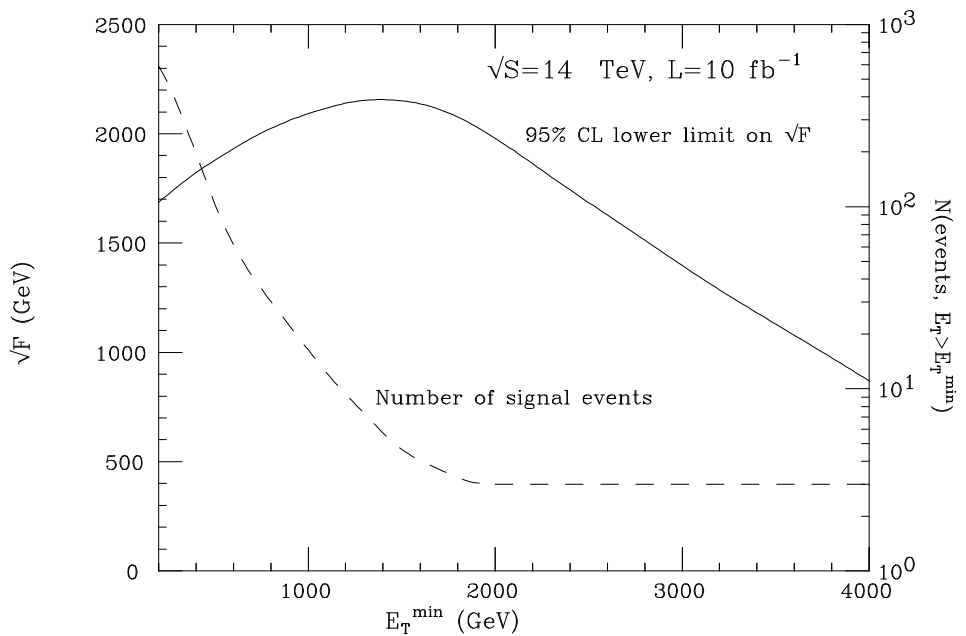


Figure 6: Same as fig. 4, for the LHC.

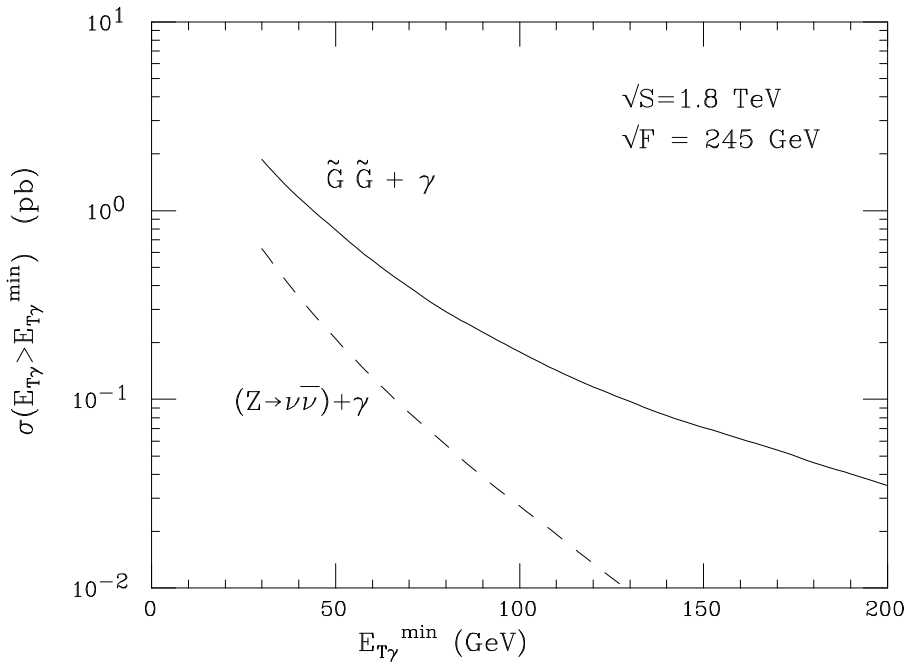


Figure 7: Production rate for $p\bar{p} \rightarrow \tilde{G}\tilde{G} + \gamma$ at $\sqrt{S} = 1.8$ TeV.

region where the background vanishes. To be conservative, we could for example decide not to use the *optimal* value of E_T^{\min} extracted from our calculation, but to choose the value of E_T above which no events are seen. This procedure would avoid reliance on the detailed prediction of the background rates. Our results indicate that the limits on \sqrt{F} would be reduced by a factor of at most 10%. Notice nevertheless that in the regions of E_T where a large background is expected, its absolute normalization can be determined with high accuracy by measuring the $(Z \rightarrow \ell^+\ell^-) + \text{jet}$ rates. In these regions of large rates, furthermore, one could use not just the total rate above a given threshold, but the highly distorted shape of the E_T -distribution as well.

5 The photon-plus-missing-energy signal

While the production rate of events with a photon plus the gravitino pair is smaller than that with a jet, the relevant source of background (associated production of $Z\gamma$) is also smaller. A recent analysis from D0 [15], for example, did not find any $\gamma + \cancel{E}_T$ event with $E_{T\gamma} > 70$ GeV in approximately 13 pb^{-1} of data. It is therefore interesting to examine the constraints on \sqrt{F} set by searches in this channel. Figure 7 shows the $\gamma + \cancel{E}_T$ signal rate, as a function of the photon E_T threshold. We chose for this plot $\sqrt{F} = 245$ GeV. In the case of photon final states, only the $q\bar{q}$ annihilation channel contributes. The results we find agree with the naive estimate:

$$\frac{\sigma(\tilde{G}\tilde{G} \gamma)}{\sigma(\tilde{G}\tilde{G} \text{ jet})} \sim \frac{Q_u^2 \alpha}{C_F \alpha_S} \sim 3\% . \quad (25)$$

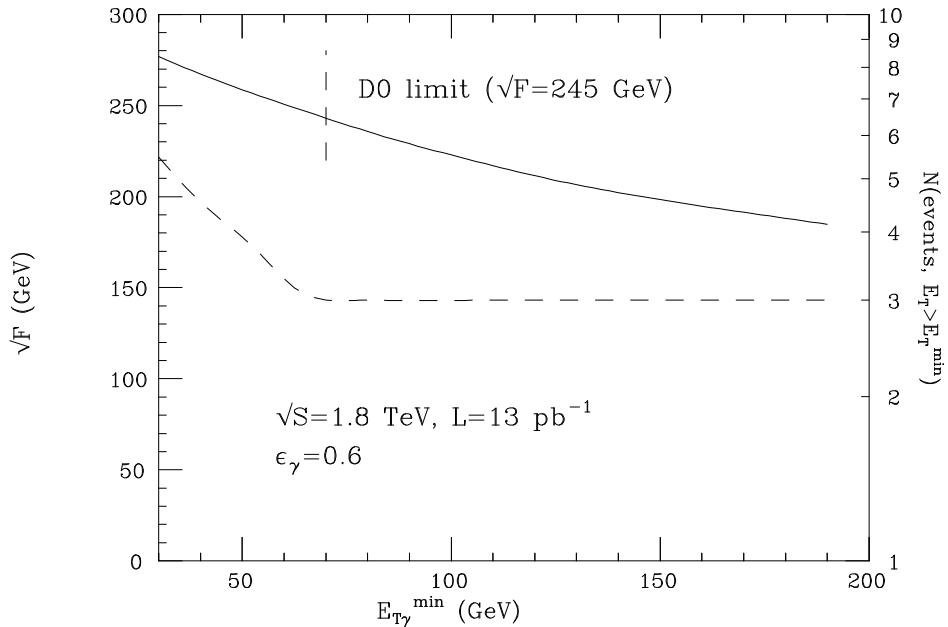


Figure 8: 95% CL exclusion limits on \sqrt{F} from the absence of $\gamma + \not{E}_T$ events at D0 [15].

The 95% CL exclusion limit on \sqrt{F} as a function of E_T^{\min} , for the 13 pb^{-1} of data corresponding to the available D0 analysis, is given in fig. 8. In addition to imposing a geometrical acceptance cut of $|\eta_\gamma| < 2.5$, we reduced both signal and background rates by the photon identification efficiency $\epsilon_\gamma = 0.6$ [15]. For $E_T^{\min} = 70 \text{ GeV}$, the threshold value above which D0 reports no events found, we obtain $\sqrt{F} > 245 \text{ GeV}$. Slightly better constraints could be obtained by using lower thresholds.

We look forward to the completion of the analyses of the full 100 pb^{-1} current data sample, for which we estimate a 95% CL limit of 290 GeV (300 GeV) for $E_T^{\min} = 70 \text{ GeV}$ (50 GeV). These numbers are only a factor of 10% worse than those obtained with the jet+ \not{E}_T analyses. Further improvements will arise from a combination of the D0 and CDF statistics.

The sensitivity achievable in the $\gamma + \not{E}_T$ channel at TeV II is displayed in figs. 9 and 10, which show the production rates and 95% CL limits after accumulation of 2 fb^{-1} of data at 2 TeV . Similar plots for the LHC are shown in figs. 11 and 12. In this case we set the photon-identification efficiency equal to 1, in the absence of a determination based on real data. While the Tevatron sensitivity in the photon channel is almost comparable to that in the jet channel, a clear advantage of the jet signal over the photon one is seen at the LHC. This is due to the smaller luminosity of the $q\bar{q}$ initial state relative to the qg initial state at the LHC.

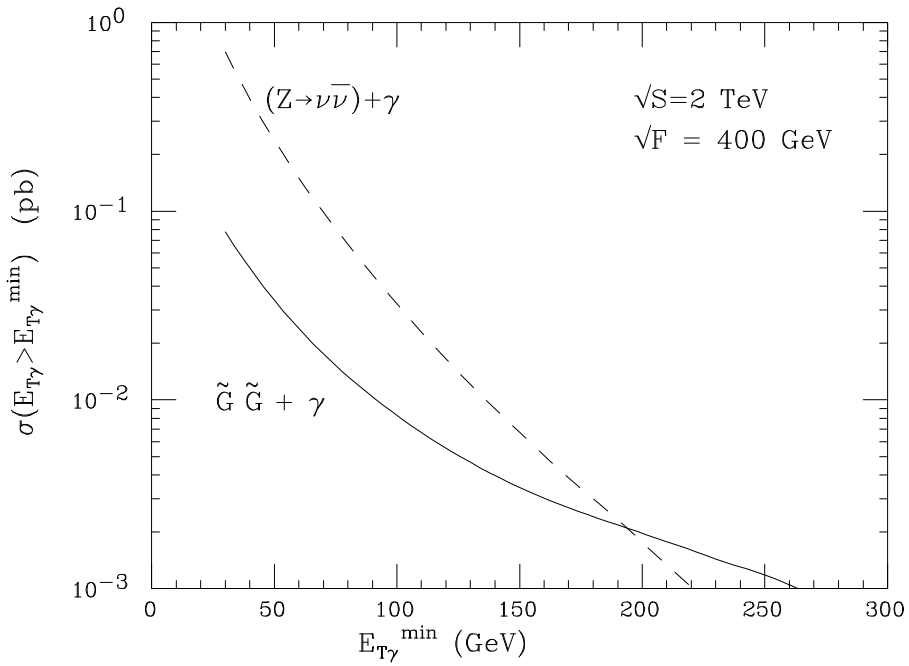


Figure 9: Production rate for $p\bar{p} \rightarrow \tilde{G}\tilde{G} + \gamma$ at $\sqrt{S} = 2$ TeV.

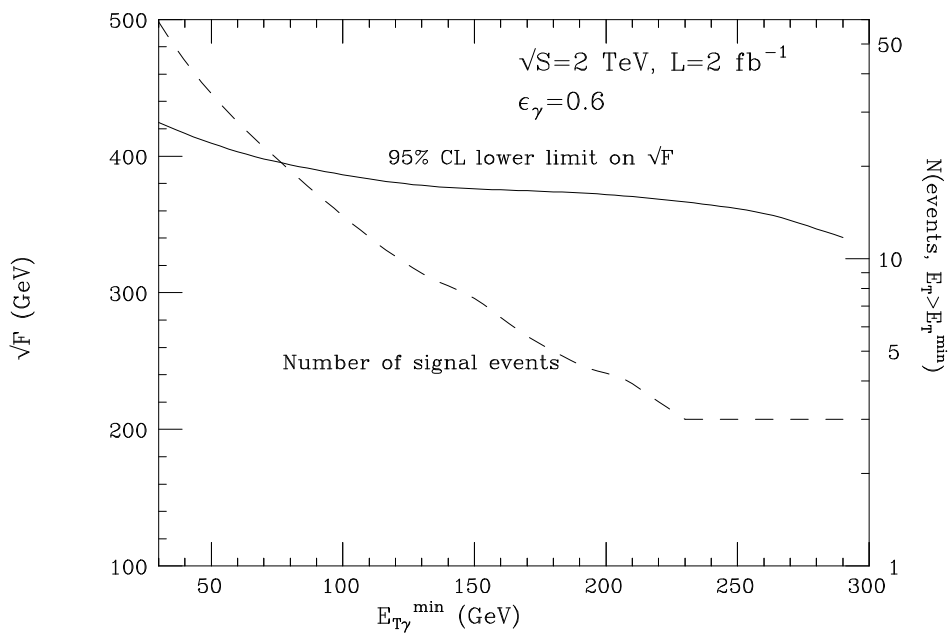


Figure 10: Solid line (scale on the left axis): estimated 95% CL exclusion limits on \sqrt{F} from the absence of a deviation from the SM $\gamma + \not{E}_T$ rate in events with $\gamma\text{-}E_T > E_T^{\min}$ at TeV II. Dashed line (scale on the right axis): number of $\tilde{G}\tilde{G} + \gamma$ events with $\gamma\text{-}E_T > E_T^{\min}$ corresponding to the 95% CL value of \sqrt{F} .

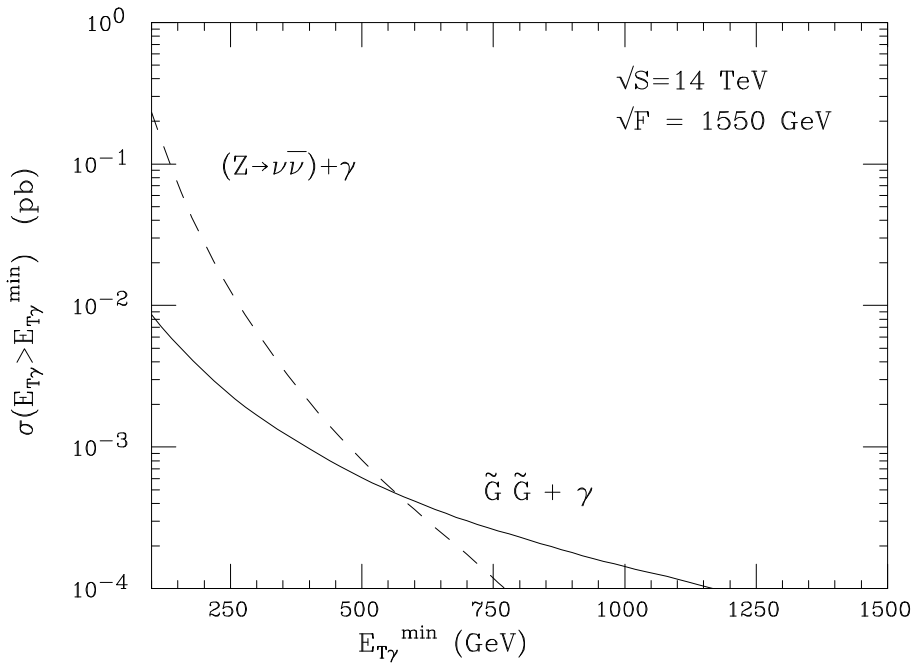


Figure 11: Production rate for $pp \rightarrow \tilde{G}\tilde{G} + \gamma$ at $\sqrt{S} = 14$ TeV.

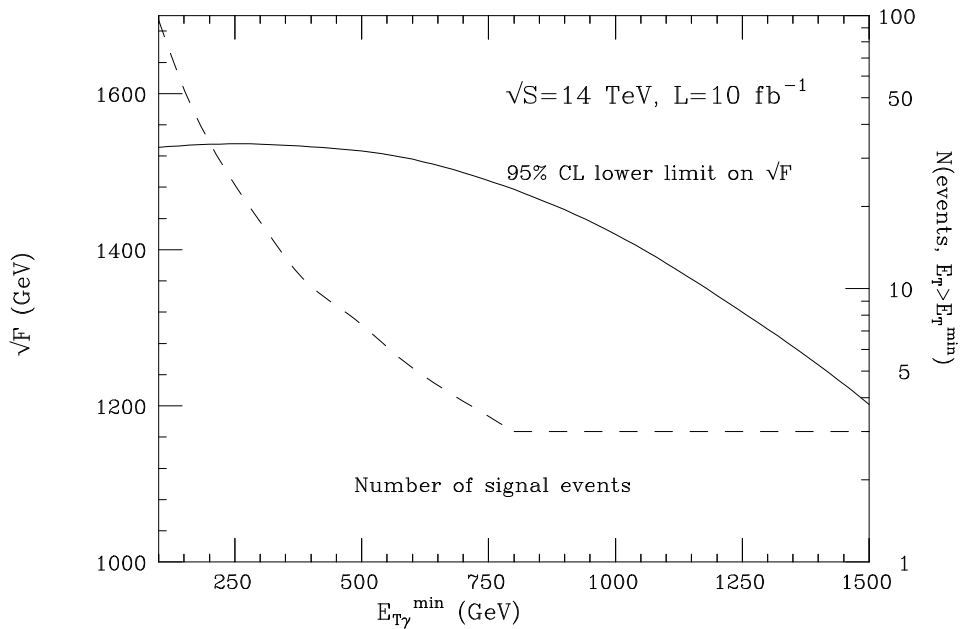


Figure 12: Solid line (scale on the left axis): estimated 95% CL exclusion limits on \sqrt{F} from the absence of a deviation from the SM $\gamma + \not{E}_T$ rate in events with $\gamma\text{-}E_T > E_T^{\min}$ at the LHC. Dashed line (scale on the right axis): number of $\tilde{G}\tilde{G} + \gamma$ events with $\gamma\text{-}E_T > E_T^{\min}$ corresponding to the 95% CL value of \sqrt{F} .

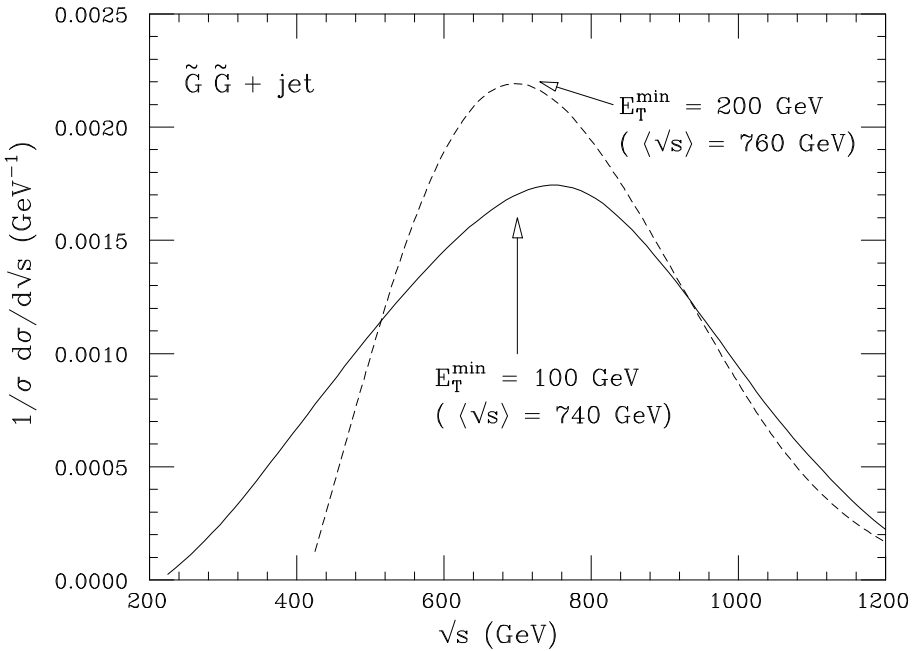


Figure 13: \sqrt{s} distribution for events with $E_T > 100$ GeV (solid line) and $E_T > 200$ GeV (dashed line) at the Tevatron.

6 Discussion and conclusions

We presented in this paper a phenomenological analysis of high-energy collider constraints on the scale of supersymmetry breaking \sqrt{F} , in one-to-one correspondence with the gravitino mass $m_{3/2}$, in models where the only light supersymmetric particle is the gravitino. A typical signature for these models is the annihilation of e^+e^- or $q\bar{q}$ pairs into gravitino pairs. To tag the events, additional emission of either a jet or a photon is necessary. The study of LEP data in ref. [5] has been extended here to signals from the Tevatron collider. The limits from the Tevatron are significantly stronger than those obtained from LEP, thanks to the higher energy reach. Supersymmetry-breaking scales as large as $\sqrt{F} = 245$ GeV ($m_{3/2} = 1.4 \times 10^{-5}$ eV) are already excluded at 95% CL by a D0 search for events with photons and missing energy. The analyses of the full TeV I data sample should increase this limit to $\sqrt{F} \simeq 300$ GeV ($m_{3/2} \simeq 2.2 \times 10^{-5}$ eV). Comparable and probably better limits should be obtained from the current data in the jet plus \not{E}_T final state, where we foresee sensitivity up to $\sqrt{F} = 335$ GeV ($m_{3/2} = 2.7 \times 10^{-5}$ eV). The upgraded Tevatron, accumulating 2 fb^{-1} at 2 TeV after the year 2000, should improve the sensitivity up to $\sqrt{F} \simeq 450$ GeV ($m_{3/2} \simeq 4.9 \times 10^{-5}$ eV). The sensitivity will then increase to $\sqrt{F} \simeq 2.2$ TeV ($m_{3/2} \simeq 1.2 \times 10^{-3}$ eV) once the LHC data become available.

These estimates have been obtained by using an effective Lagrangian containing only the degrees of freedom associated to the ordinary particles and the $\pm 1/2$ helicity states of the gravitino. Such a Lagrangian is non-renormalizable and is expected to provide a good approximation of the fundamental theory in an energy range bounded from above by a

critical value $E_c \sim (2 \div 3)\sqrt{F}$. Beyond E_c , perturbative unitarity gets violated and the non-local character of the low-energy theory should show up. These considerations also bound the mass M of the new particles called to rescue unitarity: $M \lesssim (2 \div 3)\sqrt{F}$. We should therefore check that, for each reaction considered, the typical energy \sqrt{s} probed by the partonic process remains within the allowed domain. Similarly, to be consistent, we should be able to consider superpartner masses sufficiently large to suppress direct production or large threshold effects, while remaining within a few times the supersymmetry breaking scale \sqrt{F} ².

These constraints turn out to hold for the cases considered in this paper. As an example, we show in fig. 13 the distribution of the variable \sqrt{s} for jet+ \cancel{E}_T events with $E_T^{min} = 100$ and 200 GeV at the Tevatron. The figure shows that the average value of \sqrt{s} probed by this class of events is indeed of the order of $2\sqrt{F}$, for the typical sensitivity range of $\sqrt{F} \sim 350$ GeV. We verified that similar results hold at the LHC, with average values of \sqrt{s} in the range of 4.5 TeV.

The study presented in this paper should allow experimentalists to establish absolute lower bounds on \sqrt{F} and $m_{3/2}$. Indeed, we do not expect that our bounds dissolve as the threshold for superparticle production is approached or crossed. On the contrary, in that case possibly stronger limits on the gravitino mass could be put [17] by exploiting the production of the gravitino in association with squarks and gluinos, or the production of jets in association with the spin-0 partners of the goldstino. No conclusive phenomenological study of this type has however been carried out as yet, since no experimental analyses are available of final states with one jet plus \cancel{E}_T .

The reader may have noticed that, in our analysis, all weak-interaction effects were neglected. For the signals discussed, and in the case of a goldstino neutral under the full electroweak gauge group, this is a consistent approximation: virtual W and Z exchange cannot give appreciable contributions. We may ask, however, if the associated production of a gravitino pair and a weak vector boson may lead to detectable signals. For the $\tilde{G}\tilde{G}Z$ final state, the Standard Model background (ZZ production with one of the Z decaying to a neutrino pair) is very small: only a few ZZ events have been observed up to now at TeV I. The signal, however, is also expected to be strongly suppressed with respect to the photon case, since the gain due to the coupling constant enhancement is much less than the loss due to the small leptonic branching ratio (hadronic decays suffer from severe background problems) and to the effects of the finite Z mass. For the $\tilde{G}\tilde{G}W$ final state the background is large, being dominated by production of a single off-shell W . In both cases, we expect weaker limits on \sqrt{F} and $m_{3/2}$ than the ones discussed in this paper.

We may also ask if the process $q\gamma \rightarrow \tilde{G}\tilde{G}q$, analogous to the ones considered in the present paper, may give rise to detectable signals at HERA. We studied this process in

²We recall that the complete absence of supersymmetric particles with masses below the TeV scale is generically disfavoured by naturalness considerations, even if moderate exceptions may exist. For this reason, the limit on \sqrt{F} obtained from our study of the future LHC data essentially saturates the range of applicability of our formalism. Note also that our approach does not set interesting constraints on models with gauge-mediated supersymmetry breaking (for a review see ref. [16]), in which typical superpartner masses are much smaller than \sqrt{F} , so that one is lead to set $\sqrt{F} \gtrsim 10 - 100$ TeV.

ep collisions at $\sqrt{s} = 300$ GeV. With 100 pb^{-1} , roughly corresponding to the present integrated luminosity collected by the ZEUS and H1 experiments, we found no sensitivity at HERA for values of \sqrt{F} in excess of 100 GeV.

In conclusion, we expect that hadron colliders will lead the search for a superlight gravitino in the next decade.

References

- [1] H.-P. Nilles, Phys. Rep. 110 (1984) 1;
H.E. Haber and G.L. Kane, Phys. Rep. 117 (1985) 75;
S. Ferrara, ed., *Supersymmetry* (North-Holland, Amsterdam, 1987).
- [2] A. Brignole, F. Feruglio and F. Zwirner, Nucl. Phys. B501 (1997) 332 [hep-ph/9703286].
- [3] P. Fayet, Phys. Lett. B84 (1979) 421, B86 (1979) 272, B117 (1982) 460 and B175 (1986) 471.
- [4] T. Bhattacharya and P. Roy, Phys. Rev. Lett. 59 (1987) 1517 [E: 60 (1988) 1455] and Phys. Rev. D38 (1988) 2284;
D.A. Dicus, S. Nandi and J. Woodside, Phys. Rev. D41 (1990) 2347, D43 (1991) 2951 and Phys. Lett. B258 (1991) 231;
D.A. Dicus and P. Roy, Phys. Rev. D42 (1990) 938;
J.L. Lopez, D.V. Nanopoulos and A. Zichichi, Phys. Rev. Lett. 77 (1996) 5168 and Phys. Rev. D55 (1997) 5813;
D.A. Dicus and S. Nandi, Phys. Rev. D56 (1997) 4166;
J. Kim et al., Phys. Rev. D57 (1998) 373.
- [5] A. Brignole, F. Feruglio and F. Zwirner, hep-ph/9711516, to appear in Nucl. Phys. B.
- [6] P. Fayet, Phys. Lett. B70 (1977) 461 and B86 (1979) 272;
R. Casalbuoni, S. De Curtis, D. Dominici, F. Feruglio and R. Gatto, Phys. Lett. B215 (1988) 313 and Phys. Rev. D39 (1989) 2281.
- [7] D.V. Volkov and V.P. Akulov, Phys. Lett. B46 (1973) 109;
E.A. Ivanov and A.A. Kapustnikov, J. Phys. A11 (1978) 2375;
T. Uematsu and C.K. Zachos, Nucl. Phys. B201 (1982) 250;
S. Samuel and J. Wess, Nucl. Phys. B221 (1983) 153;
J. Wess, in *Quantum Theory of Particles and Fields*, B. Jancewicz and J. Lukierski eds., (World Scientific, Singapore, 1983), p. 223;
T.E. Clark and S.T. Love, Phys. Rev. D39 (1989) 2391 and D54 (1996) 5723.
- [8] A. Brignole, F. Feruglio and F. Zwirner, JHEP 11 (1997) 001 [hep-th/9709111].
- [9] T.E. Clark, T. Lee, S.T. Love and G.-H. Wu, hep-ph/9712353.

- [10] O. Nachtmann, A. Reiter and M. Wirbel, Z. Phys. C27 (1985) 577.
- [11] M. Jamin and M.E. Lautenbacher, Comput. Phys. Commun. 74 (1993) 265.
- [12] For a review, see M.L. Mangano and S. Parke, Phys. Rep. 200 (1991) 301.
- [13] A.D. Martin, R.G. Roberts and W.J. Stirling, Phys. Lett. B387 (1996) 419.
- [14] The CDF Collaboration, Phys. Rev. Lett. 77 (1996) 448.
- [15] The D0 Collaboration, Phys. Rev. Lett. 78 (1997) 3640 and hep-ex/9710031.
- [16] G.F. Giudice and R. Rattazzi, hep-ph/9801271, submitted to Physics Reports.
- [17] See the first paper by D.A. Dicus, S. Nandi and J. Woodside in ref. [4].